SOBEL OPERATOR AND PCA FOR NEAREST TARGET OF RETINA IMAGES

B. Sivaranjani[1] and C. Kalaiselvi[2]
[1]*Department of Computer Science, Tiruppur Kumaran College for Women, India*
[2]*Department of Computer Applications, Tiruppur Kumaran College for Women, India*

Abstract

In eye, innermost layer is retina. Various important anatomical structures are available in this. Different eye diseases like diabetic retinopathy, glaucoma, etc are indicated by this. For clinical study, patient screening, and diagnosing ocular diseases, physicians are assisted by vascular intersections and blood vessels extraction in retinal images. Retina image's nearest template are detected using fuzzy neural network (FNN), Probabilistic neural network (PNN) and Adaptive Neuro Fuzzy Inference System (ANFIS) classifier's ensemble in recent work. However, various factors like low contrast are having adverse effect on image quality. Accuracy is reduced by this and it is susceptible to errors owing to different human factors. For overcoming these issues, image denoising is introduced first in this work. Clustering algorithm is used for performing this denoising. Fuzzy clustering are used for removing noises present in samples. The, Sobel edge detection operator is used for detecting edges in retina images. To enrich retina image in image enhancement, enhanced linear contrast stretching is used. Mutual Information (MI) optimization is initialized as a coarse localization process using dimension reduction, where local optima are avoided and optimization domain is narrowed down. Then, Enhanced fuzzy neural network (FNN), Improved Probabilistic neural network (PNN) and Adaptive Neuro Fuzzy Inference System (ANFIS) classifier's ensembling is used for recognizing retina image's nearest template.

Keywords:

Contrast Stretching, Diagnosing Ocular Diseases, Edge Detection, Retina Image, Eye Diseases

1. INTRODUCTION

According to the World Health Organization, 135 million people worldwide have diabetes mellitus, with the number of diabetics expected to rise to 300 million by 2025. To avert avoidable vision loss, early detection and treatment of these diseases is critical. Diabetes mellitus (DM) is a life-threatening chronic, systemic disease characterized by a disordered metabolism and abnormally high blood sugar (hyperglycemia) caused by low insulin levels with or without abnormal insulin resistance [1] [2].

It is possible to show that prevention and treatment are comparatively affordable when compared to the healthcare and rehabilitation costs associated with vision loss or blindness using computer simulations. The assessment of the risk of developing age-related macular degeneration (ARMD) necessitates the accurate detection and quantification of retinal anomalies that are thought to be disease precursors. The so-called drusen, which appear as abnormal white-yellow deposits on the retina [3] [4], are typical signs for the latter.

Currently, color retinal images are used to visually detect the presence of drusens. Because of the non-uniform lighting and the variability of the pigmentation of the background tissue, segmenting these characteristics using traditional image analysis techniques is very difficult. The quantity and quality of drusens can be determined using automated detection and analysis.

Retina image's nearest template are detected using fuzzy neural network (FNN), Probabilistic neural network (PNN) and Adaptive Neuro Fuzzy Inference System (ANFIS) classifier's ensemble in recent work. However, various factors like low contrast are having adverse effect on image quality [5] [6]. Accuracy is reduced by this and it is susceptible to errors owing to different human factors. For overcoming these issues, image denoising is introduced first in this work. Clustering algorithm is used for performing this denoising. Fuzzy clustering are used for removing noises present in samples. The, Sobel edge detection operator is used for detecting edges in retina images.

To enrich retina image in image enhancement, enhanced linear contrast stretching is used. Mutual Information (MI) optimization is initialized as a coarse localization process using dimension reduction, where local optima are avoided and optimization domain is narrowed down. Then, Enhanced fuzzy neural network (FNN), Improved Probabilistic neural network (PNN) and Adaptive Neuro Fuzzy Inference System (ANFIS) classifier's ensembling is used for recognizing retina image's nearest template [7] [8].

2. LITERATURE REVIEW

In retina images, for diseases diagnosis, various methods are used and are reviewed in this section.

For classifying abnormal (disease-infected) and normal (healthy) retinal images, an approach is proposed by Yadav and Singh [8]. It uses machine learning based retina image feature classification technique. Proposed technique's performance is 77.3%, if SVM is used. When compared with decision tree, quadratic discriminant, linear discriminant, k-NN classifier's better performance is produced by this.

Retinal vessels are used for computing CVD in a technique proposed by Rajan [9]. Disease presence are predicted using the measurements involved in this processes. Available information extraction from inside tissues is a major function in this retinal vessels. In cardiovascular diseases like glaucoma, hyper tension, blood pressure, etc, treatment and recognition, these information are used. Obtained retinal image is filtered and segmented.

Through support vector machine (SVM), for vein and arteries classification, their results are used. Cup-to-disc ratio (CDR) is computed via detection of optic disc and optic cup measurement. CVD presence is recognized using artificial neural networks (ANN) and measured its parameters. Hence, in this work, CVD presence is recognized using detected retinal images.

For segmenting retinal vessel, Extreme Learning Machine (ELM) based supervised technique is proposed by Mishra and Banerjee [10]. At first, for every fundus image pixel, vector field's divergence and Hessian, phase congruency, morphological

features, local features and 39-D discriminative feature vectors set are extracted. According to manual labels and feature vector, for training set pixel, matrix is constructed. These are given as ELM classifier's input.

Binary retinal vascular segmentation is produced as classifier's output. For removing region with less than 30 pixels and are isolated from retinal vascular, implemented an optimization processing. In retinal vessels segmentation, effectiveness of proposed technique when compared with available technique is shown in the experimentation conducted using public Digital Retinal Images for Vessel Extraction (DRIVE) database.

Javed et al. [11] showed a novel method for edge-based enhancement of retinal images in the JPEG compressed domain, which is a crucial operation for disease diagnosis. The performance of the evolved algorithm is compared to state-of-the-art methods in the uncompressed (spatial) domain in terms of both quality of enhancement and computing time, using publicly accessible retinal datasets from DRIVE and DIARETDB1.

Tuba et al. [12] suggested an overlapping-block-based algorithm for segmenting retinal blood vessels based on support vector machine classification using chromaticity and DCT coefficients as features. The proposed algorithm was validated on the DRIVE data set's standard benchmark retinal images. When the results were compared to available ground truth images and other methods from the literature, vessel segmentation was found to be exceptional in every case.

Roy et al. [13] looked at diabetic macular edema (DME), choroidal neovascularization (CNV), and drusen as three disorders. Six different convolutional neural network (CNN) architectures are used to classify these diseases. The aim is to compare the accuracy, precision, F-measure, and memory of the six different CNNs. The architectures used are either coupled with or without transfer learning, and a comparison of how the CNN architectures work with or without transfer learning has been drawn.

There was a dataset with the above-mentioned retinal disorders but no pathology. When fed multiple retinal images of different diseases, the designed models could recognize the particular disease or no pathology. As a result, the obtained results are promising and demonstrate the supremacy of the proposed model.

To distinguish blood vessels from fund us images, Guo et al. [14] suggested a supervised approach based on a multi-level convolutional neural network. Small vessels can be differentiated well and the image's global spatial consistency can be guaranteed by using both local and global feature extractors.

Meanwhile, to improve segmentation results, unsupervised pre-processing and post-processing processes are used. On the DRIVE database, experiment results show that the suggested technique outperforms the state-of-the-art performance (AUC up to >0.978).

3. PROPOSED METHODOLOGY

Detailed discussion about retina image target matching based on proposed model is presented in this section. In this model, fuzzy clustering is used in first stage for image denoising. Then

sobel edge detection operator is used for detecting retina images. In third stage, to enrich retina image, image enhancement is introduced with enhanced linear contrast stretching.

In fourth stage, Mutual Information (MI) optimization is initialized as a coarse localization process using dimension reduction, where local optima are avoided and optimization domain is narrowed down. In fifth stage, enhanced fuzzy neural network (FNN), Improved Probabilistic neural network (PNN) and Adaptive Neuro Fuzzy Inference System (ANFIS) classifier's ensembling is used for recognizing retina image's nearest template. Proposed work's overall architecture is illustrated in Fig.1.
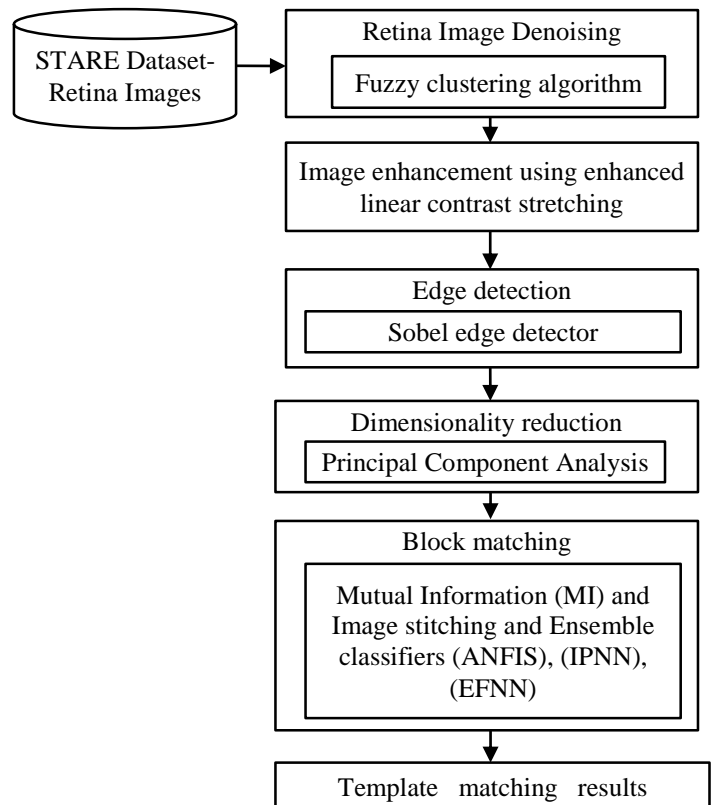
Fig.1. Overall architecture of the proposed work

3.1 NOISE REMOVAL USING FUZZY CLUSTERING

Retina Dataset: A vivo data collected using low-cost adapter (<US$400) based optical system D-eye and STARE retinal dataset are used for testing the proposed technique with synthetic deformations. Comparison is made between different dimensional reduction methods performance on STARE dataset.

Proposed flowchart on retinal image is displayed in Fig.2 which denounces fuzzy clustering usage. Identification phase defines the effectiveness of noise removal. Noisy pixel location are computed effectively using proposed detection algorithm which leads to false alarm rate maximization and miss detection rate minimization.

Using clustering, low intensity and high intensity noisy pixels are independently clustered. In noise-free group, majority pixels are clustered. In this noise removal method, in two processes, impulse noise detection is accomplished. Noisy pixels are located

at first and noise-free pixels are maintained in second phase as illustrated in Fig.2.
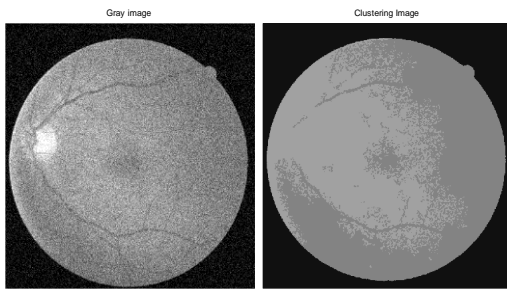
Fig.2. Fuzzy Clustering Noise removal

The step by step process of Image denoising:

Process I: Location of noisy pixels detection

Step 1: A window with $M \times N$ size is selected which is centered on every retina image's pixel.

Step 2: Central pixel's neighborhood pixels are divided into two clusters. Assume central pixel at which window is centered at $p(i,j)$ using FCM algorithm.

Step 3: After FCM application, formed two clusters are assumed as C_1 and C_2. In every cluster, maximum value available are computed after clusters formation.

Step 4: There will be $\times N = X$ values in window. These X values are divided into two clusters in unsupervised manner using FCM algorithm. In these clusters, available two maximum values are assumed as m_1 and m_2.

Step 5: In ascending order, from every cluster, m_1 and m_2 values are sorted so that $m_1 < m_2$.

Step 6: Central pixel $p(i,j)$ is classified as noisy or noise-free using following expression,

$$p(i,j) = \begin{cases} noise & if \ p(i,j) \le m_1 \\ noise\ free & if \ m_1 < p(i,j) \le m_2 \end{cases} \quad (1)$$

where, pixels in cluster with minimum intensity value m_1 is considered as noisy pixel and pixels with maximum intensity value m_2, is considered as noise free pixel.

Step 7: Pixels are left unaltered, if it lies in noise free cluster.

Step 8: In second detection stage, pixels are processed again, if it is noisy.

Process II: Location of noisy pixels detection

Step 1: Window size is changed to $U \times V$

Step 2: Up to satisfying stopping criteria, Steps 3-7 are repeated in same way.

Step 3: Pixel is marked as noisy pixel, if in second stage also, it is detected as noisy pixel, else it is marked as noise free.

Step 4: A median filter, which is well-known is used for performing noisy pixel's restoration. Within window of size $U \times V$, neighboring pixel's median value are computed and noisy pixel values are replaced using this computed value.

In next step, for edge detection process, these noiseless pixels are given as an input.

3.2 EDGE DETECTION USING SOBEL EDGE DETECTION OPERATOR

In image object recognition and segmentation, edge is a basic element.

In an image, boundaries bounded by regions are characterized using these edges. At any (x,y) co-ordinates pair, amplitude 'f' and two spatial functions $f(x,y)$ determines these edges. At this point, light depth is computed using this. Difference in image pixel intensity or discontinuities in brightness are used for analyzing edges in edge detection [15]-[17].

Edges have ramp profile and are obscure in real world image. In those conditions, edges position are thicker due to blurring effect. A discrete differentiation operator is Sobel mask. In vertical and horizontal directions, for approximate derivative values computation, two 3×3 convolution kernels are used by this operator. In horizontal of Sobel operator, at 1st and 3rd columns, in center, it has 2 and -2 values. Same values are available in vertical kernel's 1st and 3rd rows.

So, pixel values around edge region are given with more weight by Sobel operator which enhances edge intensity. The Eq.(2) and Eq.(3) are used for defining vertical and horizontal derivatives. The Eq.(3) gives edge's magnitude.

$$g_x = (z_3 + 2z_6 + z_9) - (z_1 + 2z_4 + z_7) \quad (2)$$

$$g_y = (z_7 + 2z_8 + z_9) - (z_1 + 2z_2 + z_3) \quad (3)$$

$$|G| = \sqrt{g_x^2 + g_y^2} \quad (4)$$

In Sobel operator, when compared with systems based on edge detection, image edge detection is highly effective. Input of YUV 4:2:2 format is given to Sobel Hardware filter format with required rows and columns count to mask with 3×3 matrix and produces same output format of YUV 4:2:2 which is being converted into YUV 4:4:4 format to reproduce colour components. To the next step, retina images with detected edges are given as input. The Fig.3 shows results of edge detection.
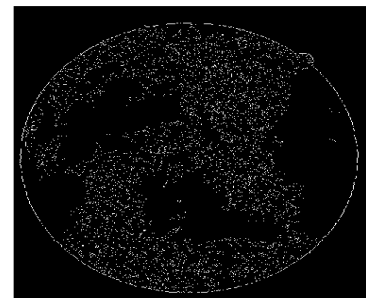
Fig.3. Sobel Edge Detection

3.3 IMAGE ENHANCEMENT USING ENHANCED LINEAR CONTRAST STRETCHING

For altering viewer's impact, image is modified using the process called enhancement. On resolving image's detection capability, contrast ratio is having strong influence. Most commonly used enhancement process corresponds to methods used to enhance image contrast. Display medium so called file's entire brightness range should be utilized for producing an image with optimum contrast ratio.

3.3.1 *Linear Contrast Stretch:*

This is also termed as contrast stretching. Noise removed WBC image's original digital values are expanded linearly into a new distribution. Within the data, more obvious subtle variations are produced by linear contrast enhancement. Images with near-Gaussian or Gaussian histograms are applied with these enhancement types. Within histogram's narrow range, all brightness values are classified and only one mode is apparent. There exist three linear contrast enhancement techniques.

For histogram stretching, images are applied with contrast stretching and image's full dynamic range is covered by this. End-in-search and basic stretching contrast are the two major contrast stretching techniques. On image, portions where all pixels concentrating in one histogram portion like middle, better performance is shown by basic stretching contrast.

To extend pixel-gray value's distribution, rectifying deficiencies and excess light in shooting process are done using contrast stretching. In general, images are classified into three classes, namely, high, normal or fine and low contrast image.

Most dark or bright image composition are used for characterizing low contrast image. In groups, some greyness degree is shown by histogram. Dark images are produced if pixels are grouped on left side and vice versa. Contrast stretching operations are used for enhancing low quality images. Following describes contrast stretching algorithm.

Step 1: Histogram of smallest to largest gray scale value (0 to 255) is scanned for computing pixel groping's lower bound and it creates first pixel which exceed predefined threshold value.

Step 2: Histogram of largest to smallest gray scale value (0 to 255) is scanned for computing pixel groping's upper bound and it creates first pixel which exceed predefined second threshold value.

Step 3: Pixels below first threshold value are assigned with 0, pixels above second threshold value are assigned with 255.

Step 4: Pixels between first threshold and second scaled threshold value for satisfying complete gray scale values range (0 to 255) with mathematical expression in Eq.(5).

$$s = \frac{r - \max}{r_{\min} - r_{\max}} \times 255 \tag{5}$$

where, original image's gray scale value is represented as r, new gray scale value is represented as s, pixel group's lowest grayscale value is represented as r_{min}, highest gray scale value is represented as r_{max}.

3.3.2 *Piecewise Linear Contrast Stretch Based On Unsharp Masking (PLCSUM):*

For leather image enhancement, piecewise Linear Contrast Stretch Based on Unsharp Masking (PLCSUM) technique is proposed in this research. A kind of image manipulation method is Unsharp masking (UM). In image, using edge contrast's small scale enhancement, detail appearances are enhanced using unsharp masking method.

Images are generally sharpened using unsharp mask. Image details and image texture are affirmed using this. Classical unsharp masking algorithm is expressed as,

$$z = n + \gamma(m-n) \tag{6}$$

where, input image is expressed as m, linear low-pass filter output is expressed as n, gain value is represented as $\hat{U}$ and $\hat{U} > 0$, this is a real scaling factor. For enhancing sharpness, signal $d = m-n$ $(\hat{U} > 1)$ is amplified often. There will be noise, image details, undershoots and over shoots at sharp edge area produced due to edge smoothing in these signals.

A visually unpleasant halo effect is used for performing over-shoot and under-shoots enhancement, if there is no possibility to perform noise enhancement. Filter which is not sensitive to smooth sharp edges and noise is required for this. Various filters like edge preserving filters, cubic filters are used in previous research works for replacing linear low-pass filters.

However, there exist some constraints in both techniques. Noise is not having any effect on cubic filter, smooth sharp edges are not produced by edge preservation filter. Thus, adaptive gain control is proposed in this work.

For leather image enhancement, an unsharp masking framework is introduced in this work. Unsharp masking algorithm which is combined with contrast stretching technique's generalization is introduced in this framework. The Fig.4 illustrates the image enhancement results.

Unsharp masking algorithm's generalization is combined with adaptive contrast stretching on halo effect issues, which are solved using an edge preserve filter forms base for this framework. Different process is used by sharpening and enhancement concept in this study and adaptive contrast stretching algorithm is used in this [17] and output is termed as $w(y)$.

The $g(d) = \hat{U}(d)d$, is used for processing image details, where, adaptive gain control is represented as d and it is a function of detail signal d's amplitude. The Eq.(7) gives the final algorithm result.

$$u = w(y) + [\gamma(d) + d] \tag{7}$$
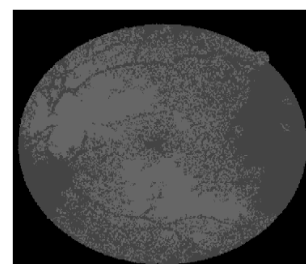
Fig.4. Image Enhancement

3.4 PCA FOR LOCATION ESTIMATION AND MUTUAL INFORMATION

This section discusses about mutual knowledge based image registration and dimensionality reduction. Low-dimensional summaries are enabled using dimension reduction techniques after image denoising while eliminating noise and redundancies in data.

In 2D space, for estimating template location, full image dimensions are duplicated, hence, template's coarse location are

added with dimensional reduction techniques. Retina Match dimension reduction technique is used in this section due to its flexible and simple nature.

Full image corresponds to mosaic image or broad-field fundus image from D-eye images. In specific, new variables range are created by PCA, as an input variable's linear combination. For multimodal image registration, MI maximization is specified after this.

Full image corresponds to mosaic image or broad-field fundus image from D-eye images. MI is maximized using optimizer which is based on Newton's approach. MI function will become a quasi-concave function and only near convergence, validity of Newton's method of parabolic theorem is accepted. On cost function's convex portion, after initial transformation, optimization is induced to get diverged.

For maximizing MI's cost function subsequently, displacement's better configuration is provided by suggested coarse localization. Computation of optimum value is similar to this and within MI metric's convex domain, it is dropped. Extreme positions are avoided and highly effective optimization is offered by this. PCA is used at first and for coarse position, blocking PCA is used, which is used for pursuing correct registration as illustrated in Fig.5.
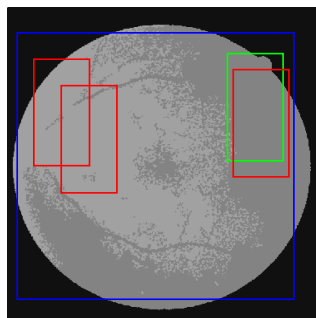
Fig.5. PCA and Coarse Localization

For accurate registration, configured the MI metric and discovers optimal transformation. Accurate registration is used for getting high efficiency and precision, after reducing optimization domain to a narrow range which is near to optimum position with coarse localization. Coarse localization is shown in Fig.5.
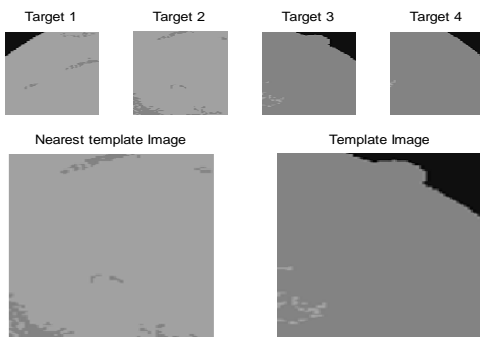
Fig.6. Coarse localization with nearest target image

3.5 PROPOSED TEMPLATE MATCHING USING ENSEMBLE CLASSIFIERS

From PCA, all images are stitched using MI for template matching and high resolution pictures are produced using image registration process. This produces enhanced diseases detection accuracy as shown in Fig.7 and 8.
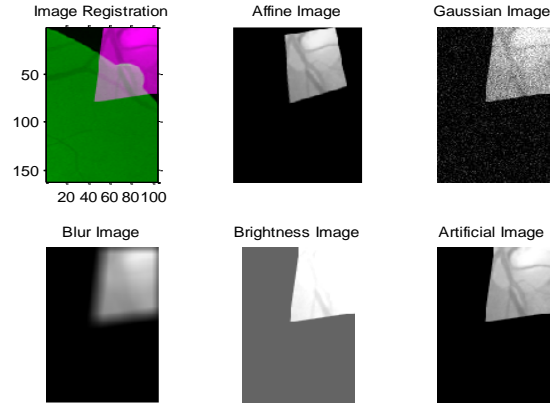
Fig.7. Image Registration
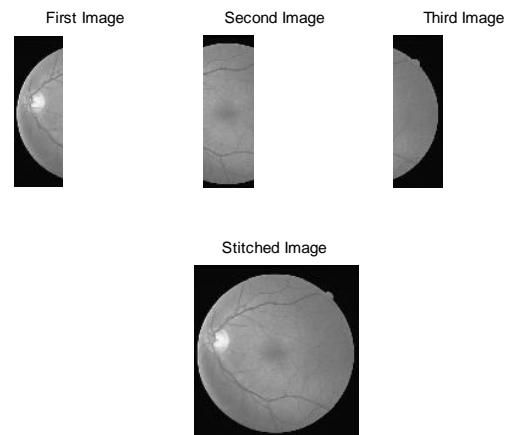
Fig.8. Image Stitching

3.5.1 Ensembling:

The thought behind all frameworks based on gathering is that on the off chance that singular classifiers or highlights are different, at that point they may produce different blunders, and consolidating these models can diminishes mistake through averaging. Troupe learning is basically used for enhancing forecast execution or order, where a solitary model doesn't have these abilities; specifically in managing multiclass issues.

In an ensemble, individual systems consequences are consolidated using different approaches. Averaging and ballot are casted using two normally utilized strategies. In Boosting gathering, in ballot casting, superior performs are shown by averaging.

Step 1: *N* specialists are generated and everyone has its own underlying qualities (From an approximation, starting qualities are arbitrarily picked)

Step 2: Every master is trained independently.

Step 3: Specialists are combined and their qualities are normalized.

In averaging strategy, i^{th} classifier is resolved in the following manner, where, for specified information x_i, ideal yield vector is represented as $d(x)$, from i^{th} arrange, genuine yield vector is represented as $f_i(x)$. In all classifiers, on first call, pictures are marked as not affected or affected. For affected images, disease grade are provided by call, vein pixels removed cotton wool spots are given as input parameters. For trained images, build models called database are build using these parts and test time's clear classification is set.

3.5.2 Adaptive Neuro Fuzzy Inference System (ANFIS):

Selected features are given as an input to ANFIS. There are various kind of neural network and it is a class of it. Its performance is based on neuro fuzzy network. ANFIS architecture implementation is shown in Fig.9 [16].

All nodes are adaptive in principal layer. Inputs fuzzy membership grade is given as an output in layer 1 and it expressed as,

$$O_i^1 = \mu_{A_i}(x) \ for \ i = 1, 2 \tag{8}$$

where, x and y represents input nodes, linguistic labels are given by A and B, membership functions are expressed as (x) and (y) and a bell shape is considered frequently by this through lowest and highest values between 0 and 1.

$$\mu(x) = \frac{1}{1 + \left(\frac{x - c_i}{a_i}\right)^{2b_i}} \tag{9}$$

Here, premise parameters set are expressed as a_i, b_i, and c_i.

There will be a fixed nodes in this subsequent layer. It is represented as M and they are used as simple multiplier. Output of this layer is expressed as,

$$O_i^2 = w_i = \mu_{A_i}(x)\mu_{B_i}(y) \quad for \ i = 1, 2 \tag{10}$$

Output w_i is expressed as rule's firing strength. Each and every node's results are used for denoting this.

There will be a fixed nodes in third layer. They are represented as N and demonstrates that they assume a normalization role for firing strengths from previous layer. This layer's output is represented using following condition.

$$O_i^3 = w_i = \frac{w_1}{w_1 + w_2} \quad for \ i = 1, 2 \tag{11}$$

Normalized firing strengths corresponds to this layer's consequences.

Nodes are adaptive in fourth layer. Each and every node's output is considered as first order polynomial and normalized firing strength (for a first order Sugeno model). This layer's output is given by this condition.

$$O_i^4 = w_i f_i = w_i \left(p_i x + q_i y + r_i \right) \tag{12}$$

where, layer 3 output is indicated as w and parameter set is given by $\{p_i, q_i, r_i\}$ and they are termed as resultant parameters.

There will be only one fixed node which termed as S in fifth layer. Every single incoming signal summation is done using this node. Henceforth, model's general output is expressed as,

$$O_i^5 = \sum_{i=1} w_i f_i = \frac{\sum_i w_i f_i}{\sum_i w_i} \tag{13}$$
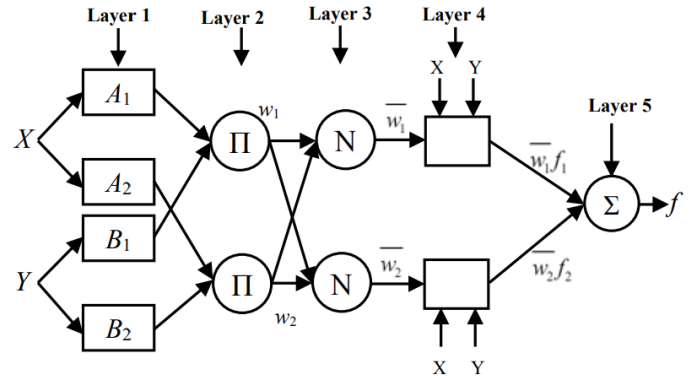
Fig.9. ANFIS architecture

Thus, an adaptive network can be produced with reason for available is identified practically with Sugeno first-order fuzzy inference system. ANFIS is streamlined using consequent and antecedent parameters modification, subsequently specific objective function's end goal can be minimized.

3.5.3 Improved Probabilistic Neural Network:

There are four network layers in improved probabilistic neural network, namely, output, summation, pattern and input layer. The Fig.10 shows basic structure of it. In network, feature vectors introduction are managed by input layer. Pattern layer's count is equal to training set's count. Between input feature vector and every training set's mode, matching relationship is computed using this layer.

Probabilities belonging to same pattern are added using summation layer. Output layer's neurons are competing neurons, which selects neurons having highest posterior probability density in all patterns as entire system's output. Network is given with training sets as input and it is trained. Data prediction is done using trained neural network. Complex back computation are not required in this feed-forward training technique, which is a major advantages of PNN [18] – [20].
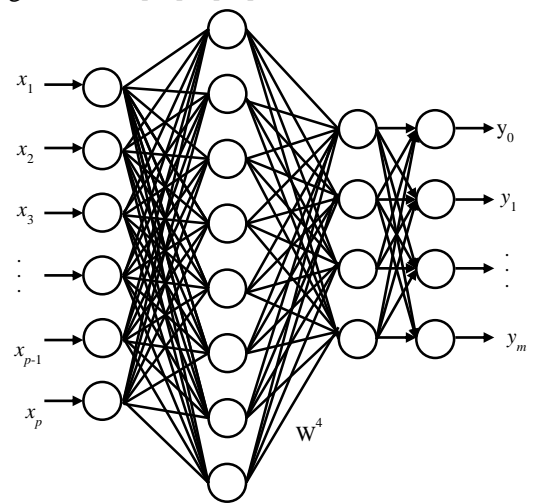
Fig.10. WPNN structure

From input layer, data $X = [x_1, x_2, \ldots, x_N]$ is transmitted directly to pattern layer's every unit when data X to be identified is input to network. Input is weighted using Euclidean distance's weighted function after receiving X in pattern layer and weighted input is obtained. Following gives of Euclidean distance expression.

$$D(i,1) = dist(IW, X) = sum\left(\left(IW(i,:) - X\right)^2\right)^{0.5} \qquad (14)$$

where, $Q \times R$ weighted matrix with training set is represented as IW, input matrix with $N \times 1$ dimension is represented as X, output matrix with $Q \times 1$ dimension is represented as D and $i = 1,2,\ldots,N$.

Pattern layer's output is computed using radial basis function after the computation of Euclidean distance. Gaussian function is considered in radial basis function.

$$radbas(n) = e^{-n^2} \qquad (15)$$

Output of pattern layer neurons are given as,

$$\hat{f}_c^p(X) = \exp\left[-\frac{\left(X - X^{(P)}\right)^T \left(X - X^{(P)}\right)}{2\delta^2}\right] \qquad (16)$$

where, pattern c's p^{th} pattern layer neuron output is represented as $\hat{f}_c^p$, $c = 1,2,\ldots,C$ data categories count is represented as C and smoothing factor is given by δ.

It is weighted probabilistic neural network. Between summation and pattern layer, weights are introduced by this and for reflecting specific pattern p's importance, weights are used from c^{th} class. Summation layer's output is modified as,

$$\hat{f}_c(X) = \sum_{P=1}^{P_c} w_c^{(P)} \exp\left[-\frac{\left(X - X^{(P)}\right)^T \left(X - X^{(P)}\right)}{2\delta^2}\right] \qquad (17)$$

where $w_c^{(P)}$ represents weight.

Pattern layer output are added using PNN's summation layer and in pattern layer, every neuron's output are not considered in this. In a weighted way, pattern layer output are added in WPNN, which is different from PNN and it considers, differences in pattern layer's output. More reasonable data dealing are done using this process in weighted summation and prediction ability are enhanced using this.

The Fig.7 shows WPNN's structure. A weight factor is multiplied with an output of pattern layer and this multiplied data is given as an input of summation layer for adding the data. There is a difference between WPNN and PNN's weighted summation technique and this technique.

3.5.4 Enhanced Fuzzy Neural Network (FNN):

The Fig.8 shows self-organizing fuzzy neural network's architecture with hierarchical pruning scheme (SOFNN-HPS). There are four layers in this architecture namely output, input, membership function (MF) and input layer. In SOFNN-HPS, proposed asymmetric Gaussian function (AGF) is used as membership function, which can rectify standard Gaussian function's symmetry constraint.

Hence, in GD-FNN, extended the ellipsoidal basis functions (EBFs) into generalized ellipsoidal basis functions (GEBFs). In input space, cluster's width flexibility can be enhanced using this. Functionality of Takagi–Sugeno–Kang (TSK) fuzzy system is equivalent to proposed SOFNN-HPS functionality and following fuzzy rules are used for describing it.

Rule j: IF x_1 is A_{1j} and . . . and x_r is A_{rj}

THEN y is w_j

where, $r(i=1,2,\ldots, r)$ and $u(j=1,2,\ldots,u)$ fuzzy IF-THEN rules. Input linguistic vector $x = [x_1, x_2,\ldots,x_r]^T$ is mapped to an output linguistic scalar y by applying fuzzy sets. In j^{th} fuzzy rule, i^{th} input variable x_i's standard fuzzy set is given by A_{ij}.

- **Input layer**: A crisp input linguistic variable is represented using every neuron in this layer. Every neuron's input is passed directly to next layer, which means that, weight adjustment is not required in this layer.

- **MF layer**: A MF is represented using every neuron in this layer for executing fuzzification operation. In GF, to eliminate symmetric width's limitation, used an AGF with dynamic width. For x_i, j^{th} AGF fuzzy set neuron's output is expressed as,

$$\mu_{ij}(x_i) = AGF(x_i; c_{ij}, \sigma_{ij}(x_i)) \qquad (18)$$

$$= \exp\left[-\frac{\left(x_i - c_{ij}\right)^2}{\sigma_{ij}^2(x_i)}\right] \qquad (19)$$

$$\sigma_{ij}(x_i) = \begin{cases} \sigma_{ij}^L & x_i \leq c_{ij} \\ \sigma_{ij}^R & x_i > c_{ij} \end{cases} \qquad (20)$$

where, for x_i, jth AGF neuron's center is represented as c_{ij}, left width is represented as σ_{ij}^L, right width is represented as σ_{ij}^R. If x_i falls on c_{ij}'s left or right side, x_i's membership function is different as shown in Eq.(2) and Eq.(3). Hence in SOFNN-HPS respective fields are generalized hyper-ellipsoidal rather than GD-FNN's hyper-ellipsoidal or D-FNN's hyper-sphere.

- **Rule Layer**: Fuzzy rule's IF-part (antecedent parameters) is represented using every neuron in this layer. Thus, fuzzy rules count is similar to neurons count in this layer. In spatial firing strength computation, if T-norm operator correspond to multiplication, j^{th} rule R_j's output can be computed as,

$$\varphi_j(X) = GEBF\left(X; C_j, \sigma_j(X)\right) \qquad (21)$$

$$= \prod_{i=1}^{r} AGF\left(X_i; C_{ij}, \sigma_{ij}(x_i)\right) \qquad (22)$$

$$= \prod_{i=1}^{r} \mu_{ij}(x_i) \qquad (23)$$

$$= \exp\left[-\sum_{i=1}^{r} \frac{\left(x_i - c_{ij}\right)^2}{\sigma_{ij}^2(x_i)}\right], \quad j = 1,2,\ldots,u \qquad (24)$$

where, j^{th} GEBF's input vector is represented as $x = [x_1, x_2,\ldots, x_r]^T$, centre vector is represented as $c_j = [c_{1j}, c_{2j},\ldots,c_{rj}]^T$ and dynamic width vector is represented as $\sigma_j(x) = [\sigma_{1j}(x_1), \sigma_{2j}(x_2),\ldots, \sigma_{rj}(x_r)]^T$. Input-output space's local expression is expressed using fuzzy rule in GEBF neuron form. AGF is introduced for constructing GEBF. Network's flexibility and learning capability can be enhanced using this.

The output layer: This layer has only one neuron for a multi-input single-output (MISO) dynamic system, which is used for representing system's output variable [21] [23]. A defuzzification operation is used for computing this layer's output. In this operation, incoming signal's weighted summation is used for computing this output and it is given by,

$$y(X) = \sum_{j=1}^{u} \omega_j \varphi_j \qquad (25)$$

where, j^{th} fuzzy rule's TSK-type THEN-part (consequent parameters) is given by w_j and it functions as input variable's polynomial. It is expressed as,

$$\omega_j = a_{0j} + a_{1j}X_1 + \cdots + a_{rj}X_r, \quad j=1,2,\ldots,u \qquad (26)$$

where, in j^{th} fuzzy rule, input variables weights are given by a_{0j}, $a_{1j},\ldots, a_{rj}$ ($j = 1, 2\ldots,u$). Therefore, there will be $1+r$ consequent weights in every fuzzy rule.

4. RESULTS AND DISCUSSION

In Retina and ASIFT match, retinal images are used for performing experimental results among four matching techniques. On four hundred source fund us image's matching image, from STARE dataset, full fund us images are retrieved as sick and strong retinas. After transforming affine to parallelogram from square, on mapping, in random selection, full fund us images are hold by every image pair.

In this area, for getting square template, squared mapped warping and cropping are performed. For 11 images, in FOV template images, attained a 200×200 pixels size. Template dimension is set as full image's 10% value. Using five image types namely, artificial, brightness, blur, Gaussian, affine, prevailing techniques like MI-ENCLA MI-ISVM, IR-MI and MI, developed Ensemble classifiers (SO-EN) Mutual Information output are analyzed. The Fig.11 shows the retina image input with Nearest Template and Target image.

Input image   Target image and nearest template
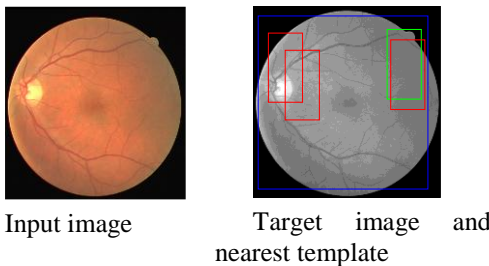
Fig.11. Retina image with Target Image and Nearest Template

Table.1. Performance comparison results for different methods

Metrics	MI	IR-MI	MI-SVM	CA-EN	SO-EN
Affine	63	76.5	85.5	89	91
Gaussian	52.5	81	90	93	95.2
Blur	70	81	90	92.7	94.1
Brightness	63	81	90	93	95
Artificial	70	90	94.5	96.2	97.5
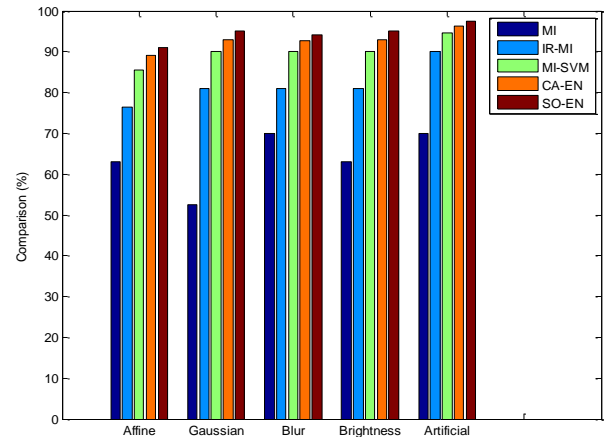
Fig.12. Different retina images matching Comparison vs. Classifiers

The Fig.12 shows comparison between available MI-ENCLA, MI-ISVM, IR-MI, MI and proposed SO-EN Retina template recognition techniques with respect to artificial images matching, brightness, blur, Gaussian and Affine.

Techniques like MI- ENCLA, MI-ISVM, IR-MI, MI produces low artificial, brightness, blur, Gaussian and affine results, while proposed novel SO-EN technique produces high artificial, brightness, blur, Gaussian and affine results as revealed in that figure. For affine image, 91% accuracy is produced by proposed SO-EN technique which is a higher value when compared with 89% accuracy of MI- ENCLA, 85.5% of MI-ISVM, 75% of IR-MI and 63% of MI.

5. CONCLUSION AND FUTURE WORK

For retina image target pattern matching, an enhanced framework is provided in this work. In this framework, fuzzy clustering is used for removing noises available in samples. Then Sobel edge detection operator is used for detecting retina image edges. To enrich retina image in image enhancement, introduced an enhanced linear contrast stretching. The Mutual Information (MI) optimization is initialized as a coarse localization process by dimension reduction. Local optima are avoided and optimization domain is narrowed using this.

The enhanced FNN, PNN and ANFIS classifier's ensemble are used for performing retinal image nearest template. With respect to artificial images matching, brightness, blur, Gaussian and Affine, better results are provided by proposed model as shown in experimental results. However, there is an accuracy issues in this method. So, other techniques can be used in future.

REFERENCES

[1] R. Deepa and N.K. Narayanan, "Detection of Microaneurysm in Retina Image using Machine Learning Approach", *Proceedings of International Conference on Innovative Trends in Information* Technology, pp. 1-5, 2020.

[2] D. Xiao, S. Yu and Y. Kanagasingam, "Retinal Hemorrhage Detection by Rule-Based and Machine Learning Approach",

Proceedings of International Conference on Engineering in Medicine and Biology Society, pp. 660-663, 2017.

[3] Y. Gao, X. Yu and C. Wu, "Automated Segmentation of the Optic Disc from Retinal Image using Modified Local Intensity Clustering Model", *Proceedings of International Conference on Chinese Control and Decision*, pp. 602-606, 2019.

[4] C. Zhu, B. Zou and R. Zhao, "Retinal Vessel Segmentation in Colour Fundus Images using Extreme Learning Machine", *Computerized Medical Imaging and Graphics*, Vol. 55, pp. 68-77, 2017.

[5] K. Wisaeng and W. Sa Ngiamvibool, "Exudates Detection using Morphology Mean Shift Algorithm in Retinal Images", *IEEE Access*, Vol. 7, pp. 11946-11958, 2019.

[6] C. Saravanabhavan, T. Saravanan, D.B. Mariappan, S. Nagaraj and K.M. Baalamurugan, "Data Mining Model for Chronic Kidney Risks Prediction Based on Using NB-CbH", *Proceedings of IEEE International Conference on Advance Computing and Innovative Technologies in Engineering*, pp. 1023-1026, 2021.

[7] P. Mehta, C. Petersen and J.C. Wen, "Automated Detection of Glaucoma with Interpretable Machine Learning using Clinical Data and Multi-Modal Retinal Images", *American Journal of Ophthalmology*, Vol. 19, No. 2, pp. 1-20, 2020.

[8] P. Yadav and N.P. Singh, "Classification of Normal and Abnormal Retinal Images by using Feature-Based Machine Learning Approach", *Proceedings of International Conference on Recent Trends in Communication, Computing, and Electronics*, pp. 387-396, 2019.

[9] S.P. Rajan, "Recognition of Cardiovascular Diseases through Retinal Images using Optic Cup to Optic Disc Ratio", *Pattern Recognition and Image Analysis*, Vol. 30, No. 2, pp. 256-263, 2020.

[10] S. Mishra and M. Banerjee, "Automatic Caption Generation of Retinal Diseases with Self-trained RNN Merge Model, *Proceedings of International Conference on Advanced Computing and Systems for Security*, pp. 1-10, 2020.

[11] M. Javed, P. Nagabhushan, B.B. Chaudhuri and S.K. Singh, "Edge Based Enhancement of Retinal Images using an Efficient JPEG-Compressed Domain Technique", *Journal of Intelligent and Fuzzy Systems*, Vol. 36, No. 1, pp. 541-556, 2019.

[12] E. Tuba, L. Mrkela and M. Tuba, "Retinal Blood Vessel Segmentation by Support Vector Machine Classification", *Proceedings of International Conference on Radioelektronika*, pp. 1-6, 2017.

[13] K. Roy, S.S. Chaudhuri and P. Roy, P., Chatterjee, "Transfer Learning Coupled Convolution Neural Networks in Detecting Retinal Diseases using OCT Images", *Proceedings of International Conference on Intelligent Computing: Image Processing Based Applications*, pp. 153-173, 2020.

[14] J. Guo, S. Ren, Y. Shi and H. Wang, "Automatic Retinal Blood Vessel Segmentation based on Multi-Level Convolutional Neural Network", *Proceedings of International Congress on Image and Signal Processing, BioMedical Engineering and Informatics*, pp. 1-5, 2018.

[15] K. Goel, M. Sehrawat and A. Agarwal, "Finding the Optimal Threshold Values for Edge Detection of Digital Images and Comparing among Bacterial Foraging Algorithm, Canny and Sobel Edge Detector", *Proceedings of International Conference on Computing, Communication and Automation*, pp. 1076-1080, 2017.

[16] S. Israni and S. Jain, "Edge Detection of License Plate using Sobel Operator", *Proceedings of International Conference on Electrical, Electronics, and Optimization Techniques*, pp. 3561-3563, 2016.

[17] N. Mathur, S. Mathur and D. Mathur, "A Novel Approach to Improve Sobel Edge Detector", *Procedia Computer Science*, Vol. 93, pp. 431-438, 2016.

[18] M.G. Raman, N. Somu and A.P. Mathur, "Anomaly Detection in Critical Infrastructure using Probabilistic Neural Network", *Proceedings of International Conference on Applications and Techniques in Information Security*, pp. 129-141, 2019.

[19] Y. Sun and J. Chen, "Indoor Sound Source Localization with Probabilistic Neural Network", *IEEE Transactions on Industrial Electronics*, Vol. 65, No. 8, pp. 6403-6413, 2017.

[20] R.K.V. Bhupatiraju and V.S.S.S.S. Dhanikonda, "Transient- and Probabilistic Neural Network-Based Fault Classification in EHV Three-Terminal Lines", *Turkish Journal of Electrical Engineering & Computer Sciences*, Vol. 26, No. 2, pp. 974-986, 2018.

[21] H.G. Han, X.L. Wu and Z. Liu, "Design of Self-Organizing Intelligent Controller using Fuzzy Neural Network", *IEEE Transactions on Fuzzy Systems*, Vol. 26, No. 5, pp. 3097-3111, 2017.

[22] J. Fei and D. Cao, "Adaptive Fractional Terminal Sliding Mode Controller for Active Power Filter using Fuzzy-Neural-Network", *Proceedings of International Conference on Knowledge and Systems Engineering*, pp. 118-122, 2018.

[23] A. Sharifian and M.J. Ghadi, "A New Method based on Type-2 Fuzzy Neural Network for Accurate Wind Power Forecasting under Uncertain Data", *Renewable Energy*, Vol. 120, pp. 220-230, 2018.